High performance organic photovoltaic cells with blade-coated active layers

Siew-Lay Lim [a], En-Chen Chen [b], Chun-Yu Chen [b], Kok-Haw Ong [a], Zhi-Kuan Chen *,[a], Hsin-Fei Meng **,[b]

[a] Institute of Materials Research & Engineering, 3 Research Link, Singapore 117602, Singapore
[b] Institute of Physics, National Chiao Tung University, 1001 Ta-Hsueh Road, Hsinchu 300, Taiwan ROC

ARTICLE INFO

ABSTRACT

High performance bulk heterojunction organic photovoltaic (OPV) cells with blade-coated active layers of POD2T-DTBT blended with [6,6]-phenyl-C71-butyric acid methyl ester (PC71BM) are demonstrated in this work. The blade-coated cells exhibit power conversion efficiencies of up to 6.74%, which is comparable to those of conventional spincoated cells but obtained with just a fraction of the material amount used for spincoating. The choice of solvent and the process conditions are manipulated to achieve dense, well-separated morphology which increases the interfacial area for charge dissociation in the blend film. The blade coating technique can be applied in the fabrication of large area, high performance OPV cells with highly efficient materials usage.

© 2012 Elsevier B.V. All rights reserved.

1. Introduction

Organic bulk heterojunction photovoltaic (PV) cells are promising renewable energy alternatives as they can be fabricated entirely by solution processing with low energy consumption. Light-weight and versatile products, such as portable battery chargers and window shades in building integrated photovoltaic applications, can be produced by low cost manufacturing through large-area printing on flexible substrates. Power conversion efficiencies (PCEs) exceeding 7% based on bulk heterojunctions have been reported along side rapid developments in the field of conjugated polymers [1–3]. We are approaching the PCE milestone of 10% at which the commercialization of this technology will be extremely attractive. The active layers of such high performance cells, consisting of new polymeric materials in blends with commercial (6,6)-phenyl-C_{61}-butyric acid methyl ester ($PC_{61}BM$) or (6,6)-phenyl-C_{71}-butyric acid methyl ester ($PC_{71}BM$), are usually deposited by spincoating, a standard method to produce uniform coatings of desired thicknesses. It allows control of the film morphology by varying the solvent system, the spinning rate and spinning time and the discrete nature of the method allows easy incorporation of treatment or processing step during film deposition. For instance, a wet film can be obtained by using a short spin time and dried slowly in a

covered petridish to achieve the effects of solvent annealing. However, the high materials wastage of more than 90% for spincoating means that materials costs are likely to escalate as the film-coated area becomes larger [4]. Existing large-area coating methods such as blade coating and slot-die coating are compatible with high speed, high volume and low cost roll-to-roll production envisioned for the scale-up and commercialization of organic photovoltaic (OPV) cells and the importance of such techniques in future manufacturing activities can be expected [5]. In encouraging developments for OPV commercialization, the operational stability of OPV cells have improved significantly in recent years [6] and OPV modules have been successfully produced by full roll-to-roll processes and integrated in practical applications [7,8].

Besides the development of large-area coating for OPV manufacturing, the design and synthesis of high performance materials with good processability for ink formulations is equally important. Uniformity, surface roughness and the resultant morphology of the blend films have to be controlled by judicious selection of process conditions and solvent systems [9]. Efforts to apply large area coating techniques have focused mainly on the bulk heterojunction blend of commercial materials poly(3-hexylthiophene) and $PC_{61}BM$. PCEs of about 4% have been achieved via blade coating of P3HT:PCBM blends using solvents such as xylene [10] and toluene [11]. Similar efficiencies have been achieved via inkjet printing [12,13], screen printing [14] and spray coating [15,16]. Some techniques such as blade coating [11,17] as well as roller painting [18] have resulted in efficiencies higher than those obtained by spincoating. The use of such techniques in place of spincoating has resulted in modified morphologies and structuring of the blend films, sometimes

---

* Corresponding author. Tel.: +65 6874 4331; fax: +65 6872 0785.
** Corresponding author. Tel.:+886 03 573 1955; fax: +886 03 573 6012.
E-mail addresses: limsl@imre.a-star.edu.sg (S.-L. Lim),
d9763818@oz.nthu.edu.tw (E.-C. Chen), ua0114@yahoo.com.tw (C.-Y. Chen),
ongkh@imre.a-star.edu.sg (K.-H. Ong), zk-chen@imre.a-star.edu.sg (Z.-K. Chen),
meng@mail.nctu.edu.tw (H.-F. Meng).

requiring the use of high boiling point additives or a co-solvent [19] in the ink formulations to enhance device efficiencies.

While materials such as poly(3-hexylthiophene) and poly(-thiophene)s have been widely used for large-area printing as well as roll-to-roll processes, as described in the previous paragraphs, no one has investigated the use of high performance OPV materials for large-area printing techniques which are scalable to roll-to-roll process. In this work, the blend of a novel, easily processible low bandgap p-type polymer POD2T-DTBT (structure as shown in Fig. 2(a)) with $PC_{71}BM$ was deposited by simple, high throughput blade coating on ITO-glass to form the active layer of an OPV cell. The hole-transporting material, poly(3,4-ethylene-dioxythiophene): poly(styrenesulfonate) (PEDOT:PSS), was deposited by spincoating prior to the blade coating process. Uniform films of the active layer in dimensions of approximately 5 cm × 7 cm were obtained with low materials wastage of less than 5%. Laboratory scale test cells with an active area of 0.04 cm^2 fabricated from such large-area active layer coatings show excellent cell efficiencies up to 6.74%, without the need for any solvent additive or post-treatment. The efficiency obtained is thus far the highest reported for cells with active layers deposited by large-area coating techniques and is on par with that obtained by conventional discrete spincoating.

2. Materials and methods

Glass/ITO substrates ($\sim 10\,\Omega/\square$) were sequentially patterned lithographically, cleaned with ultrasonication in detergent, deionised water, acetone and isopropyl alcohol, and dried at 80 °C for 1 h. After UV–ozone treatment, a 40 nm PEDOT:PSS (CLEVIOS P VP Al 4083) film is spincoated on the ITO substrate and annealed at 120 °C for 10 min.

POD2T-DTBT was synthesized as reported [20]. $PC_{71}BM$ was purchased from Nano-C. The solution blends of POD2T-DTBT:$PC_{71}BM$ (1:1 w/w) were prepared in anhydrous 1,2-dichlorobenzene (DCB, Aldrich) and chlorobenzene (CB, Aldrich). The final concentration of the polymer in the blend was 10 mg/ml. For spincoated devices, the blend solution was spincoated onto the PEDOT:PSS-coated ITO-glass at 800 rpm for 40 s in an inert atmosphere. The blend film was slowly dried in a covered petridish. For the blade-coated sample using DCB solution, the wet polymer film was coated on PEDOT:PSS-coated ITO-glass by a blade-coater with a blade gap of 60 μm and a blade speed of about 15 cm/s. This was followed immediately by spinning the sample at 800 rpm for 40 s. Rapid-drying blade coating from CB solution is performed on a hot plate at 80 °C with a blade gap of 60 μm and a blade speed of about 40 cm/s. Hot wind from a hair dryer is applied to enhance the drying and uniformity. Dry films are obtained in seconds. The thicknesses of the blend films obtained from the above processes are about 100–110 nm. The blade coating process was carried out in an inert atmosphere.

100 nm of aluminum was deposited by thermal evaporation to form the cathode, followed by post-annealing at 120 °C for 10 min. The structure of the bulk heterojunction OPV cell was ITO/PEDOT:PSS/POD2T-DTBT:$PC_{71}BM$/Al and each cell had an active area of 0.04 cm^2.

All the cells were packaged in the glove box and measured in the ambient environment. The power conversion efficiency was measured by the solar simulator (PEC-L11, Peccell Technologies) under AM1.5G irradiation. The external quantum efficiency (EQE) was measured by the spectral response measurement system (SR300, Optosolar GMBH). The morphology of the blend film was monitored by atomic force microscope (AFM, Dimension 3100, Digital Instruments). The UV–visible absorption spectra of the blend films were measured by Agilent 8453 UV–visible spectrophotometer.

3. Results and discussion

The novel p-type polymeric semiconductor POD2T-DTBT has demonstrated high performance in OPV cells due to its low bandgap and high mobility [20]. It was found that the best cell efficiency was obtained with 1,2-dichlorobenzene (DCB) as solvent, with solvent annealing during the film drying process. The high boiling point of DCB (180 °C) allows the formation of a phase-separated, nanofibrous polymer network in the blend film during solvent annealing, thus enhancing charge transport in the device. The best spincoated cell (**DCB-spin**) shows a power conversion efficiency (PCE) of 6.77%, with an open-circuit voltage (V_{oc}) of 0.769 V, fill factor (FF) of 0.653 and short-circuit current (J_{sc}) of 13.49 mA/cm^2, with PCEs ranging from 6.47% to 6.77% for cells from the same batch (Table 1). All fabricated cells have an active area of 0.04 cm^2.

Based on these excellent results, DCB was used in the blade coating process to prepare large area films on substrates with dimensions of approximately 5 cm × 7 cm. Blade coating at room temperature followed by slow drying of the wet blade-coated film was attempted to mimic the solvent annealing process used for the spincoated film. However, due to the high boiling point of DCB, uniform films could not be obtained by this process. The wet blade-coated film was thus spun dry to improve uniformity. With this technique, PCEs ranging from 4.85% to 5.27% can be obtained, with the best cell (**DCB-blade and spin**) showing a PCE of 5.27%, with V_{oc} of 0.750 V, FF of 0.655, and J_{sc} of 10.73 mA/cm^2.

Although good results were obtained with DCB as the solvent, the need for the wet blade-coated film to be spun dry would limit the size of substrate coated and was incompatible with the roll-to-roll process. To improve film uniformity and speed up the drying process, a solvent with a lower boiling point, chlorobenzene (CB, boiling point=131 °C), was used and blade coating was done on a substrate heated at 80 °C instead of the room temperature conditions used previously. POD2T-DTBT shows

Table 1

Average photovoltaic properties and their standard deviations for 4–8 cells from the same large area blend film, and equivalent circuit model parameters for the best cells prepared with different solvents and processes. All cells have an active area of 0.04 cm^2.

Cell [a]	V_{oc} (V)	J_{sc} (mA/cm^2)	FF	PCE ($_{max}$) (%)	R_{sh}[b] (kΩ cm^2)	R_s[b] (kΩ cm^2)	n[b]	J_0[b] (mA/cm^2)
DCB-spin	0.765 ± 0.003	13.16 ± 0.26	0.658 ± 0.003	6.62 ± 0.12 (6.77)	1105	4.4	1.36	6.88×10^{-9}
DCB-blade and spin	0.747 ± 0.002	10.31 ± 0.31	0.648 ± 0.004	4.99 ± 0.19 (5.27)	1095	4.9	1.40	1.23×10^{-8}
CB-spin	0.733 ± 0.003	10.48 ± 0.09	0.562 ± 0.009	4.32 ± 0.05 (4.36)	629	8.2	1.58	4.11×10^{-8}
CB-blade (80 nm)	0.769 ± 0.005	13.88 ± 0.11	0.608 ± 0.008	6.49 ± 0.16 (6.69)	692	7.4	1.59	3.09×10^{-8}
CB-blade (110 nm)	0.765 ± 0.003	13.35 ± 0.79	0.594 ± 0.034	6.07 ± 0.71 (6.74)	666	7.5	1.52	1.25×10^{-8}
CB-blade (135 nm)	0.759 ± 0.004	12.85 ± 0.65	0.566 ± 0.031	5.54 ± 0.59 (6.15)	674	8.5	1.57	2.73×10^{-8}

[a] DCB: 1,2-dichlorobenzene, CB: chlorobenzene, spin: spincoating, blade: blade coating, blade and spin: combination of spincoating and blade coating.

[b] R_{sh}: shunt resistance, R_s: series resistance, n=diode ideality factor, J_0: reverse saturation current density.

good solubility in CB and films 100–110 nm thick can be prepared from CB solutions by both spincoating and blade-coating. The best blade-coated cell (**CB-blade**) yields an exceptional PCE of 6.74%, with V_{oc} of 0.768 V, FF of 0.622, and J_{sc} of 14.11 mA/cm^2. This high efficiency is on par with the performance of the **DCB-spin** cell with solvent annealing. A comparison with the photovoltaic properties of the **DCB-spin** cell shows that while V_{oc} remains almost unchanged, J_{sc} is enhanced and FF is reduced for **CB-blade** cell. The best spincoated cell (**CB-spin**) shows a poorer PCE of 4.36%, with V_{oc} of 0.739 V, FF of 0.559, and J_{sc} of 10.55 mA/cm^2 All the cell parameters, including V_{oc}, J_{sc} and FF, are lowered relative to the **DCB-spin** cell. The use of a different solvent affects the morphology of the blend film and is likely to be the cause of the poorer performance. Overall, the shunt resistances (R_{sh}) for cells fabricated from CB solutions are lower at 629–692 kΩ cm^2 compared to 1095–1105 kΩ cm^2 for device fabricated from DCB solutions, indicating higher degrees of charge recombination in the blend films. The corresponding series resistances (R_s) are higher at 7.4–8.2 kΩ cm^2 compared to 4.4–4.9 kΩ cm^2, for films of similar thicknesses, and are representative of higher bulk resistances in the blend films (Table 1).

The blade coating process can be controlled to produce films of different thicknesses. Cells with active layer thicknesses of about 80 nm and 135 nm were also fabricated. The best cell with 80 nm active layer yields a comparably high PCE of 6.69%, with V_{oc} of 0.773 V, FF of 0.619, and J_{sc} of 13.98 mA/cm^2, while the best cell with a 135 nm active layer has a slightly lower PCE of 6.15%, with V_{oc} of 0.761 V, FF of 0.593, and J_{sc} of 13.62 mA/cm^2. The current density–voltage characteristics (Fig. 1(b)) show that decreases in J_{sc} and FF are the main reasons for the lower average PCEs with increasing film thicknesses. This can be attributed to the non-optimal morphology and the higher R_s. Larger deviations in the cell parameters are also observed due to the challenge of ensuring uniform drying for thicker films. Nevertheless, a reliable method of fabricating cells via blade coating that allows PCEs of more than 6% to be obtained easily, with a comfortable tolerance for film thicknesses between 80 nm and 110 nm, has been successfully demonstrated.

It is intriguing that high performance blade-coated cells can be fabricated using CB solution blends, with just seconds for film formation and drying, when spincoated cells using such blends show poorer performance. Furthermore, the blade coating process is distinctly different from the solvent annealing process used for DCB solutions blends, where film formation and drying takes more than 2 h. Similar observations have also been reported for P3HT:PCBM blends, whereby cells fabricated by blade coating of toluene solutions shows higher PCE than those using DCB solutions, although the converse is observed for spincoating [11]. The good results have been attributed to the ability of the donor and

acceptor to quickly self-assemble into the desired ordered and interpenetrating morphology during the blade coating process in the absence of centrifugal force.

The physics of the separation of photogenerated charges in an organic solar cell can be analyzed through the evaluation of two diode parameters, the ideality factor n and the reverse saturation current density J_0 using the equivalent circuit model, following the implementation of classic photovoltaic theory in organic solar cells [21]. These parameters can be extracted from the dark J–V characteristics of the cells. n is indicative of the internal morphology of the bulk heterojunction, by reflecting the density of interfaces where recombination can occur, and is expected to be of similar values for films processed from the same solvent. n is also strongly related to the contacting of the individual components within the blend by the electrode materials. From the data, n is about 1.36 and 1.40 for the **DCB-spin** and **DCB-blade and spin** cells, respectively. Although the two different processing methods have not yielded significantly different morphologies, dark current analysis shows that the device behavior of the **DCB-spin** cell is closer to the ideal diode behavior.

J_0 is the diode current around zero bias and indicates the number of charges able to overcome the energetic barrier in the reverse direction. It represents the minority charge density in the vicinity of the barrier, which, in this case, is at the donor/acceptor interface in the bulk heterojunction and is related to the nanoscale phase separation between the donor and the acceptor. J_0 for the **DCB-spin** cell is lower by approximately a factor of 2 compared to the **DCB-blade and spin** cell, which can indicate a larger degree of phase separation of the two components. Such a reduction in J_0 has the expected effect of increasing the V_{oc} of the **DCB-spin** cell by about 18 mV [10].

Cells fabricated from CB solutions show higher n and J_0 values compared to those fabricated from DCB solutions. Different ideality factors can be expected due to the change of solvent and the higher n is a manifestation of the lower fill factor and increased recombination. Comparing the processes, the n of 1.58 and J_0 of 4.11×10^{-8} mA/cm^2 for the **CB-spin** cell are reduced to 1.52 and 1.25×10^{-8} mA/cm^2, respectively, for the **CB-blade** cell. The J_0 for **CB-blade** cell is lower by more than a factor of 3 and V_{oc} higher by about 30 mV compared to the **CB-spin** cell.

Analysis of the external quantum efficiency (EQE) measurements shows that the **DCB-spin** and **CB-blade** cells have similar maximum EQEs of 0.65–0.68 at wavelengths of 450–460 nm (Fig. 2(c)). However, the **CB-blade** cell has distinctly more efficient photocurrent generation at wavelengths between 550 nm and 700 nm. Absorption in this region can be attributed to the polymer POD2T-DTBT and the EQE spectrum is indicative of a greater contribution to the photocurrent generation by the POD2T-DTBT component. Theoretical short-circuit currents obtained by
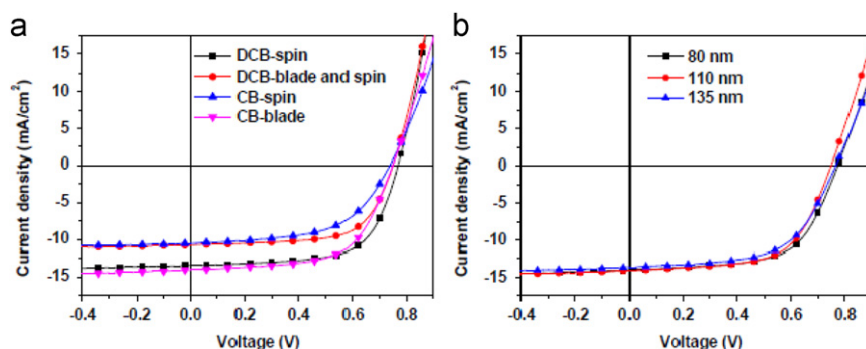
Fig. 1. Current density–voltage characteristics of the best POD2T-DTBT:PC71BM cells fabricated (a) using different solvents and processes (**DCB-spin**: 1,2-dichlorobenzene (DCB) and spincoating, **DCB-blade and spin**: DCB and a combination of spincoating and blade coating, **CB-spin**: chlorobenzene (CB) and spincoating, **CB-blade**: CB and blade coating) and (b) using CB and blade coating with resultant active layers' thicknesses of 80 nm, 110 nm and 135 nm.
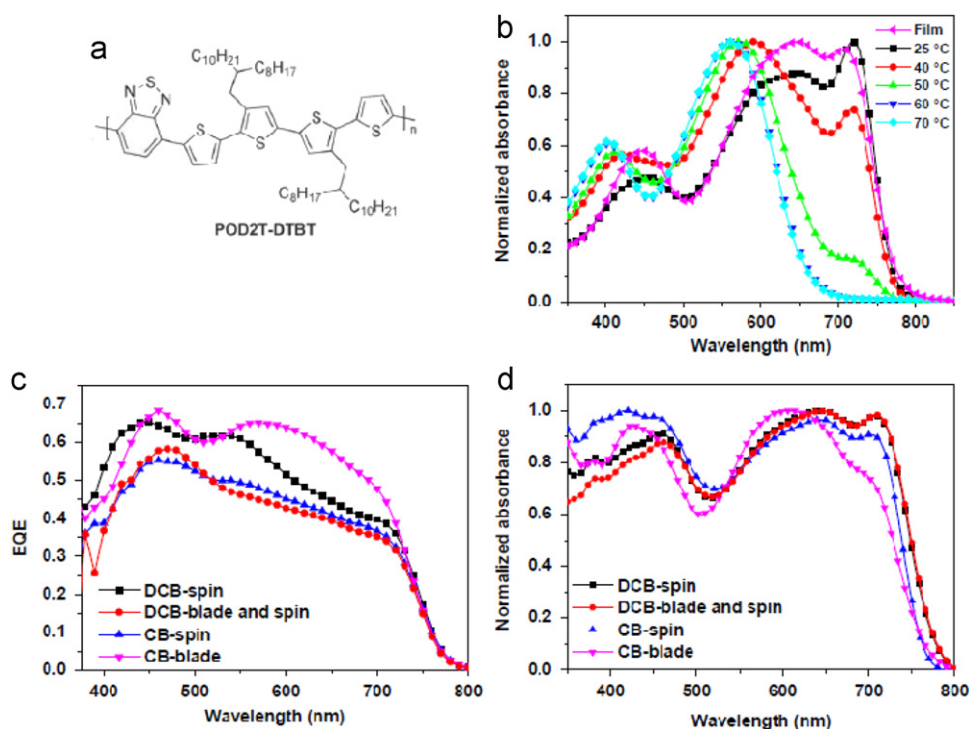
Fig. 2. (a) Molecular structure of POD2T-DTBT, (b) UV–visible absorption spectra of POD2T-DTBT in thin film, and in 1,2-dichlorobenzene solution at different temperatures, (c) external quantum efficiencies (EQE) of the best cells fabricated with different solvents and processes, and (d) UV–visible absorption spectra of the blend films prepared with different solvents and processes.

integrating the EQE spectra are in good agreement with the experimental currents, with deviations of less than 6%.

Differences in the solvent system and coating methods influence the resultant film morphologies significantly. The boiling point of the solvent affects the evaporation rate, and therefore the time available for self-organization and nanophase separation in the blend film. The coating method also affects the drying rate. The effects of these factors on the resultant films were investigated via UV–visible spectroscopy and atomic force microscopy (AFM). Fig. 2(d) shows the normalized UV–visible absorption spectra of films prepared by different coating processes using different solvents. The absorption spectra of both **DCB-spin** and **DCB-blade and spin** are largely similar, with peaks at around 645 nm and 708 nm in the longer wavelength region. The two peaks are associated with π–π stacking and aggregate absorption. Thus, the different coating processes do not affect the extent of polymer stacking and aggregation significantly when DCB is the solvent. However, distinct differences due to changes in processing are observed when CB is the solvent. While the absorption spectrum of the **CB-spin** film also shows a π–π absorption peak at around 645 nm and a blueshift aggregation absorption peak at around 702 nm, the aggregation absorption peak is reduced to a shoulder at around 698 nm for the **CB-blade** film, with a huge blueshift of the π–π absorption peak to around 607 nm and the appearance of another peak at around 426 nm. Similar spectral changes are obtained when the polymer, dissolved in DCB, is heated above room temperature (Fig. 2(b)). These observations indicate a significant reduction in the extent of polymer stacking and aggregation in the **CB-blade** film. From the EQE and absorption measurements, photocurrent generation is increased despite the reduced aggregation in the **CB-blade** film.

Comparing the surface morphologies of films obtained using the same technique of spincoating but with different solvents (Fig. 3(a) and (c)), fine phase separation and the formation of a nanofibrous network are observed for the **DCB-spin** film (root-mean-square roughness, R_q=1.4 nm), while larger aggregated domains, up to 100 nm in size, are easily observed for the **CB-spin** film (R_q=2.5 nm). The shorter exciton diffusion length, larger interfacial area for charge separation and better charge transport network resulted in significantly higher J_{sc} and FF in the **DCB-spin** cell, indicating DCB as the solvent of choice when blend films are deposited by spincoating.

The AFM image of the **DCB-blade and spin** film (R_q=1.7 nm) (Fig. 3(b)) shows shorter and less interconnected polymer nanofibers than those in the **DCB-spin** film. The solvent annealing process allows a higher degree of freedom and more time for self-organization and phase separation in the film, but is not adopted during blade coating due to non-uniform drying and dewetting of the wet polymer film. A separate experiment shows that slow drying of the blend film enhances J_{sc} by up to 5–6%, compared to the fast drying process, for devices fabricated from films of similar thicknesses. The morphology of the **DCB-blade and spin** film may be enhanced by solvent vapour annealing of the dry film with 1,2-dichlorobenzene for a few hours in place of solvent annealing. However, such treatment is not compatible with the roll-to-roll process.

The **CB-blade** film surface reveals the formation of finer and more evenly distributed polymer domains, with a lower R_q of 0.7 nm, as shown in Fig. 3(d). Although there is no obvious nanofibrous network as observed for the **DCB-spin** surface, a dense phase-separated interpenetrating network with fine dimensions is clearly present. Such morphology provides a smaller exciton diffusion length as well as increased donor–acceptor interfacial area, providing the two-fold benefits of reducing the exciton recombination and increasing the area for charge separation in the blend. The high J_{sc} of 14.11 mA/cm^2 observed for the best **CB-blade** cell can be attributed to the favourable blend morphology. The blade-coated film dries swiftly in seconds on the 80 °C hotplate, limiting the growth in feature size as there is less time for the formation of polymer nanofibers
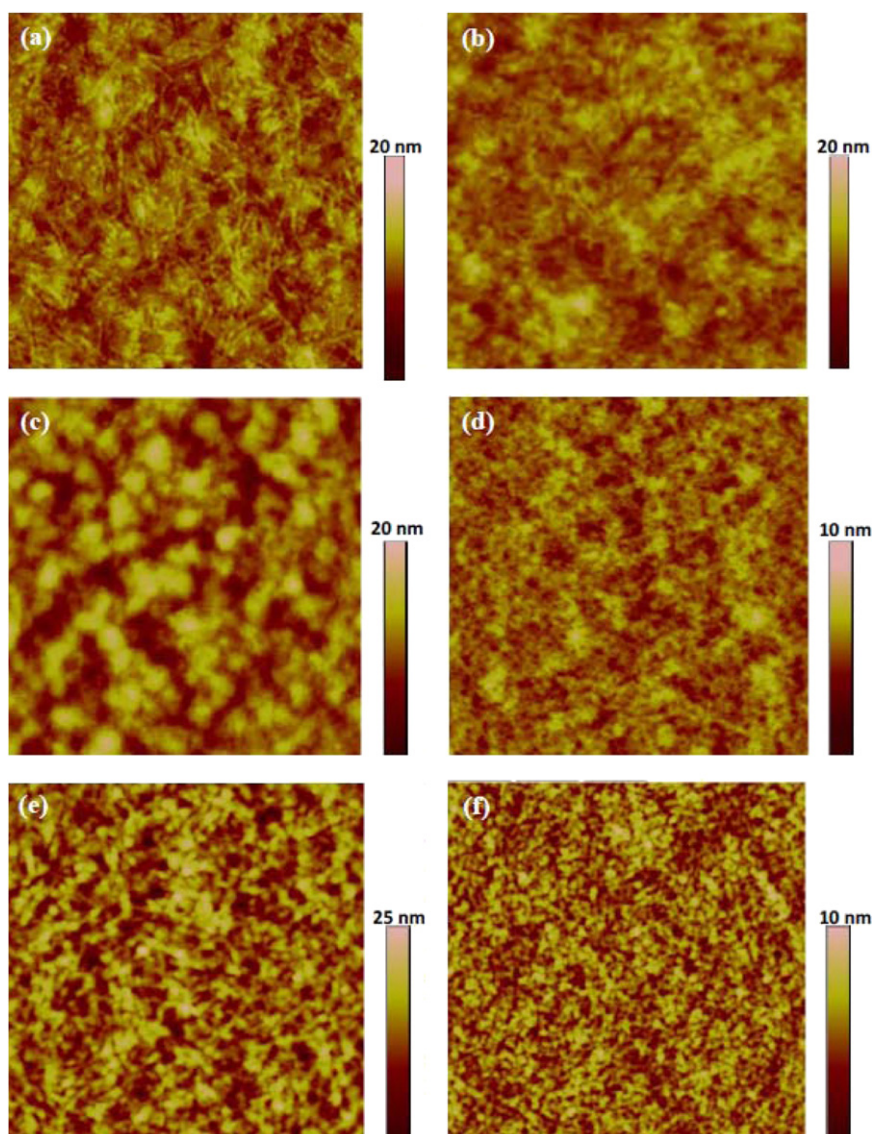
Fig. 3. Atomic force microscopy (AFM) height images of the blend films (a) **DCB-spin**, (b) **DCB-blade and spin**, (c) **CB-spin**, (d) **CB-blade**, (e) **DCB-spin** with PCBM removed and (f) **CB-blade** with PCBM removed. All images are 2 μm × 2 μm.

or PCBM crystallites. The blade coating process is controlled to yield fine and well-distributed polymer domains.

To allow closer examination of the polymer network formed in **DCB-spin** and **CB-blade** films, the PCBM on the film surface was removed by rinsing with alkanethiol for a few seconds. The respective AFM images are shown in Fig. 3(e) and (f). The higher density, uniformity and smaller dimensions of the polymer network in the **CB-blade** film is apparent, while the **DCB-spin** film is less dense, with a larger distribution of feature sizes and bigger voids remaining after the removal of PCBM. The growth and distribution of polymer and PCBM domains in the blend film have therefore been effectively constrained in the blade-coated film.

The efficient charge transport network of the **DCB-spin** film results in low bulk resistance (R_s), high shunt resistance (R_{sh}) and, therefore, high efficiency in the fabricated cell. In comparison, the R_s and R_{sh} of the **CB-blade** cell are much less indicative of high cell efficiency. In particular, the R_s of the **CB-blade** cell remains high in spite of the smaller polymer domain size. From UV-visible absorption measurements, we have found that the extent of polymer aggregation is reduced in the **CB-blade** film. This may result in lower hole mobility of the polymer in the **CB-blade** film,

compared to hole transport along polymer nanofibers of larger dimensions in the **DCB-spin** film, thus increasing the bulk resistance. The lower R_{sh} can be attributed to recombinative losses due to the less interconnected transport pathways formed during the swift drying process of the **CB-blade** film, compared to the more extensive nanofibrous network of the **DCB-spin** film. Besides bulk resistance of the film, R_s of the cell is also dependent on other factors such as interfacial resistance, for example, at the organic-metal interface. Such factors probably do not have a significant effect in this case due to the similar cell structure and post-annealing conditions used.

Thus, our work shows that the increased interfacial area for charge dissociation, due to phase separation, results in more efficient photocurrent generation by the polymer in the blend and is the overriding factor for the excellent photovoltaic performance in the **CB-blade** cell, despite the less favorable diode characteristics and resistances. While the use of DCB solution at room temperature requires a combination of spincoating and blade coating to obtain uniform films, a change of solvent to CB coupled with substrate heating allows the active layer of an OPV cell to be deposited rapidly by blade coating only. Despite the

small active areas used in photovoltaic characterization, the rapid blade coating-only process developed in this work can be incorporated readily with current OPV module designs [22,23] to form the active layers of large-area OPV modules. Other considerations for future large-area fabrication include the use of more environmentally friendly, non-chlorinated solvents for depositing the active layers [24], reducing the power loss due to the finite sheet resistance of ITO [25] and the use of techniques such as laser ablation, in place of wet chemical etching, to increase the proportion of the substrate area utilized as active area [26].

4. Conclusions

In summary, highly efficient OPV cells, with efficiencies above 6%, based on our novel p-type polymer POD2T-DTBT were fabricated by blade coating. The high throughput coating process was simple with low materials wastage. Large-area coatings with high performance in cells were obtained by the use of an alternative solvent and careful control of the coating conditions. The domain size was effectively constrained to produce fine phase separation and thus large interfacial area for exciton dissociation in the blend film for high J_{sc}. The best cell efficiencies with small active areas were on par with those of similar cells fabricated by conventional spincoating. Our work demonstrated the potential of incorporating both the material POD2T-DTBT and the blade coating technique into low-cost roll-to-roll manufacturing of OPV cells for practical applications. We are one of the first to use a high performance material different from poly(3-hexylthiophene) for large-area printing and with resulting cell efficiencies higher than those for poly(3-hexylthiophene). The findings of this work are important for our extension of blade coating to the fabrication of cells with larger active and substrate areas. We will also be investigating the use of non-chlorinated, less toxic solvents in view of larger scale applications in the future.

References

[1] Y. Liang, Z. Xu, J. Xia, S.T. Tsai, Y. Wu, G. Li, C. Ray, L. Yu, For the bright future —bulk heterojunction polymer solar cells with power conversion efficiency of 7.4%, Advanced Materials 22 (2010) E135–E138.

[2] T.Y. Chu, J. Lu, S. Beaupre, Y. Zhang, J.R. Pouliot, S. Wakim, J. Zhou, M. Leclerc, Z. Li, J. Ding, Y. Tao, Bulk heterojunction solar cells using thieno[3,4-c]pyrrole-4,6-dione and dithieno[3,2-b:2′,3′-d]silole copolymer with a power conversion efficiency of 7.3%, Journal of the American Chemical Society 133 (2011) 4250–4253.

[3] S.C. Price, A.C. Stuart, L. Yang, H. Zhou, W. You, Fluorine substituted conjugated polymer of medium band gap yields 7% efficiency in polymer—fullerene solar cells, Journal of the American Chemical Society 133 (2011) 4625–4631.

[4] J.J. Licari, Coating Materials for Electronic Applications—Polymers, Processes, Reliability, Testing, Noyes Publications/William Andrew, Inc., New York, 2003.

[5] F.C. Krebs, T. Tromholt, M. Jørgensen, Upscaling of polymer solar cell fabrication using full roll-to-roll processing, Nanoscale 2 (2010) 873–886.

[6] M. Jørgensen, K. Norrman, S.A. Gevorgyan, T. Tromholt, B. Andreasen, F.C. Krebs, Stability of polymer solar cells, Advanced Materials 24 (2012) 580–612.

[7] F.C. Krebs, J. Fyenbo, M. Jørgensen, Product integration of compact roll-to-roll processed polymer solar cell modules: methods and manufacture using flexographic printing, slot-die coating and rotary screen printing, Journal of Materials Chemistry 20 (2010) 8994–9001.

[8] F.C. Krebs, J. Fyenbo, D.M. Tanenbaum, S.A. Gevorgyan, R. Andriessen, N. van Remoortere, Y. Galagan, M. Jørgensen, The OE-A OPV demonstrator anno domini 2011, Energy and Environmental Science 4 (2011) 4116–4123.

[9] Y. Yao, J. Hou, Z. Xu, G. Li, Y. Yang, Effects of solvent mixtures on the nanoscale phase separation in polymer solar cells, Advanced Functional Materials 18 (2008) 1783–1789.

[10] P. Schilinsky, C. Waldauf, C.J. Brabec, Performance analysis of printed bulk heterojunction solar cells, Advanced Functional Materials 16 (2006) 1669–1672.

[11] Y.H. Chang, S.R. Tseng, C.Y. Chen, H.F. Meng, E.C. Chen, S.F. Horng, C.S. Hsu, Polymer solar cell by blade coating, Organic Electronics 10 (2009) 741–746.

[12] S.H. Eom, H. Park, S.H. Mujawar, S.C. Yoon, S.S. Kim, S.I. Na, S.J. Kang, D. Khim, D.Y. Kim, S.H. Lee, High efficiency polymer solar cells via sequential inkjet-printing of PEDOT:PSS and P3HT:PCBM inks with additives, Organic Electronics 11 (2010) 1516–1522.

[13] C.N. Hoth, P. Schilinsky, S.A. Choulis, C.J. Brabec, Printing highly efficient organic solar cells, Nano Letters 8 (2008) 2806–2813.

[14] S.E. Shaheen, R. Radspinner, N. Peyghambarian, G.E. Jabbour, Fabrication of bulk heterojunction plastic solar cells by screen printing, Applied Physics Letters 79 (2001) 2996–2998.

[15] C. Girotto, D. Moia, B.P. Rand, P. Heremans, High-performance organic solar cells with spray-coated hole-transport and active layers, Advanced Functional Materials 21 (2011) 64–72.

[16] S.Y. Park, Y.J. Kang, S. Lee, D.G. Kim, J.K. Kim, J.H. Kim, J.W. Kang, Spray-coated organic solar cells with large-area of 12.25 cm^2, Solar Energy Materials and Solar Cells 95 (2011) 852–855.

[17] C.N. Hoth, S.A. Choulis, P. Schilinsky, C.J. Brabec, On the effect of poly(3-hexylthiophene) regioregularity on inkjet printed organic solar cells, Journal of Materials Chemistry 19 (2009) 5398–5404.

[18] J.W. Jung, W.H. Jo, Annealing-free high efficiency and large area polymer solar cells fabricated by a roller painting process, Advanced Functional Materials 20 (2010) 2355–2363.

[19] A. Lange, M. Wegener, C. Boeffel, B. Fischer, A. Wedel, D. Neher, A new approach to the solvent system for inkjet-printed P3HT:PCBM solar cells and its use in devices with printed passive and active layers, Solar Energy Materials and Solar Cells 94 (2010) 1816–1821.

[20] K.H. Ong, S.L. Lim, H.S. Tan, H.K. Wong, J. Li, Z. Ma, L.C.H. Moh, S.H. Lim, J.C. de Mello, Z.K. Chen, A versatile low bandgap polymer for air-stable, high-mobility field-effect transistors and efficient polymer solar cells, Advanced Materials 23 (2011) 1409–1413.

[21] C. Waldauf, M.C. Scharber, P. Schilinsky, J.A. Hauch, C.J. Brabec, Physics of organic bulk heterojunction devices for photovoltaic applications, Journal of Applied Physics 99 (2006) 104503-1–104503-6.

[22] J.E. Lewis, E. Lafalce, P. Toglia, X. Jiang, Over 30% transparency large area inverted organic solar array by spray, Solar Energy Materials and Solar Cells 95 (2011) 2816–2822.

[23] R. Tipnis, J. Bernkopf, S. Jia, J. Krieg, S. Li, M. Storch, D. Laird, Large-area organic photovoltaic module-fabrication and performance, Solar Energy Materials and Solar Cells 93 (2009) 442–446.

[24] Y. Galagan, I.G. de Vries, A.P. Langen, R. Andriessen, W.J.H. Verhees, S.C. Veenstra, J.M. Kroon, Technology development for roll-to-roll production of organic photovoltaics, Chemical Engineering and Processing 50 (2011) 454–461.

[25] B. Muhsin, J. Renz, K.-H. Drüe, G. Gobsch, H. Hoppe, Efficient polymer solar cell modules, Synthetic Metals 159 (2009) 2358–2361.

[26] S. Choi, W.J. Potscavage, B. Kippelen, Area-scaling of organic solar cells, Journal of Applied Physics 106 (2009) 054507-1–054507-10.